

# RELATION U-NET

Sheng He, Rina Bao, P. Ellen Grant, Yangming Ou

Boston Children’s Hospital, Harvard Medical School

## ABSTRACT

Towards clinical interpretations, this paper presents a new “output-with-confidence” segmentation neural network with multiple input images and multiple output segmentation maps and their pairwise relations. A confidence score of the test image without ground-truth can be estimated from the difference among the estimated relation maps. We evaluate the method based on the widely used vanilla U-Net for segmentation and our new model is named Relation U-Net which can output segmentation maps of the input images as well as an estimated confidence score of the test image without ground-truth. Experimental results on four public datasets show that Relation U-Net can not only provide better accuracy than vanilla U-Net but also estimate a confidence score which is linearly correlated to the segmentation accuracy on test images.

**Index Terms**— Relation U-Net, deep relation learning, medical image segmentation, confidence score estimation

## 1. INTRODUCTION

Many deep learning-based methods for medical image segmentation [1] have been proposed to improve the accuracy. Most deep learning models are “output-only” models, which only output a single segmentation map given the input image. In general, the average accuracy on the evaluation dataset is reported. However, in practice the average accuracy on the evaluation dataset does not mean that every test image has the same or similar accuracy, especially the test images sampled from the clinical practice. Some test images are easy samples with high quality while some test images are difficult samples with smooth boundaries, poor contrast or small size of the target regions with high uncertainty [2]. Thus, deploying the trained model in clinical practice requires an interactive interpretation or post-correction of the segmentation outputs to automatically identify a subset of the difficult testing samples for experts inspection [3]. There is an unmet need to evaluate segmentation accuracies and even to reject failed segmentation when, in real-world applications, the ground-truth is often unavailable.

To address this problem, an “output-with-confidence” model is required in real-world applications. It needs to automatically rank the test samples without ground-truth by the difficulty or the confidence score of segmentation on each

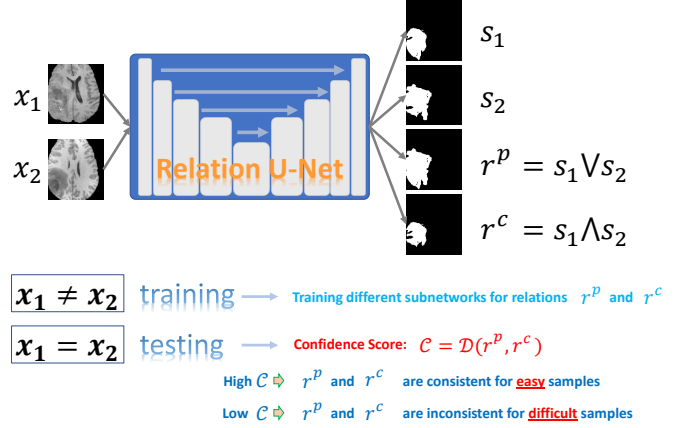


Fig. 1. Illustration of the proposed Relation U-net.

sample image. Based on the rank list, end users can select the more challenging testing samples for further inspection [3], which can save the human annotation and auditing time.

In this paper, we propose an example of the “output-with-confidence” model based on the popular U-Net for segmentation, named Relation U-Net (Fig. 1). It is a generalization of the vanilla U-Net and Fig. 2 shows the main difference between them. The proposed Relation U-Net receives two input images and outputs four segmentation maps including the segmentation of each input image and their corresponding relations. During testing, the two input images can be sampled from the same input image and the discrepancy of the estimated relation segmentation maps is correlated to the segmentation accuracy of each test images. Thus, the discrepancy of the estimated relation segmentation maps can be considered as a confidence score which can be used to rank the test images for the end users to inspect and review the difficult samples.

## 2. METHOD

### 2.1. Relation U-Net

Fig. 1 shows the framework of the Relation U-Net. Given two different input images  $x_i$ ,  $i = 1, 2$  their corresponding binarized segmentation maps  $s_i$  in the training set, we use logical operations to define the relations based on segmentation maps

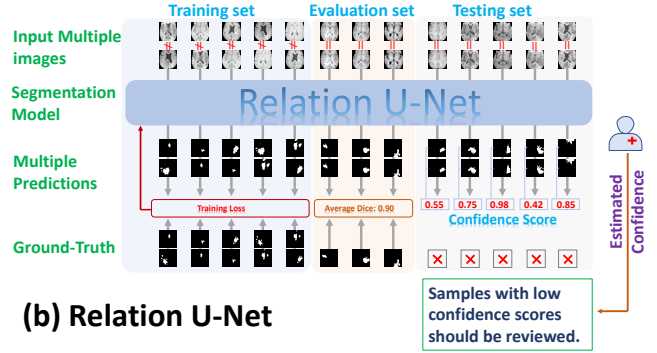
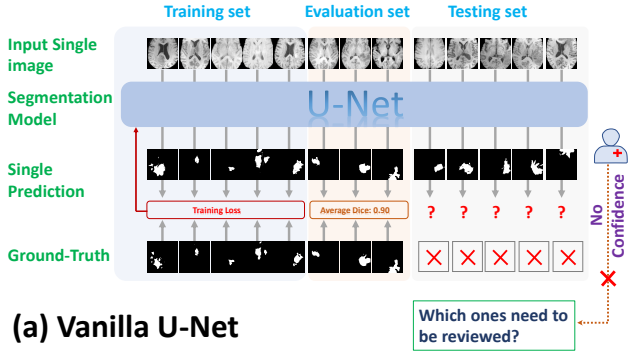


Fig. 2. The comparison of the vanilla U-Net (a) and the proposed Relation U-Net (b). (Zoom in for a better visualization)

$s_i$ , similar to studies [4]. Two relations are considered in this paper, including the *Possible* (union)  $r^p = s_1 \vee s_2$  and *Consensus* (intersection)  $r^c = s_1 \wedge s_2$  relations between the segmentation maps  $s_1$  and  $s_2$  of two different images  $x_1$  and  $x_2$ . The *Possible* relation map captures the pixels/voxels that have been segmented as belonging to the target in at least one image. The *Consensus* relation map represents the pixels/voxels that have been segmented as belonging to the target object in both images.

### 2.2. The structure of neural network

In this paper, we use the multiple-input multiple-output (MIMO) configuration [4, 5] to build Relation U-Net. We use the popular U-Net [1] as the baseline which only requires two changes. At the input layer, the two input images are concatenated. Since we need four outputs (see Fig. 2), at the last layer, four different predictions are obtained by adding four different classifiers.

The Relation U-Net takes two inputs and returns four outputs including the estimated segmentation  $s_i$  for the input images and their corresponding relations  $r^p$  and  $r^c$ . During training, the two inputs are sampled independently from the training set and the four different classifiers for segmentation are trained based on the ground-truth of corresponding labels. Thus, the Relation U-Net does not only learn the information for each input image, but also learns the relations among the pairs of samples. At test time, the multiple input images can be sampled from different images or the same input image is repeated two times to feed into the Relation U-Net, which can make four independent segmentation maps.

### 2.3. Estimating of Confidence Score

Based on the definition, the *Possible*  $r^p$  and *Consensus*  $r^c$  relations are reflexive [4], indicating that when the pair of input images  $x_1, x_2$  are from the same sample  $x_1 = x_2$ , the output of the relations  $r^p$  and  $r^c$  is the same to the segmentation of the input:  $r^p = s^c = s_1 = s_2$ . However, since

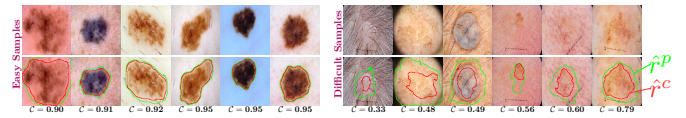


Fig. 3. Examples of images on the ISIC2018 dataset with relation segmentation maps:  $\hat{r}^p$  (green contours) and  $\hat{r}^c$  (red contours). The  $\hat{r}^p$  and  $\hat{r}^c$  are the same on easy samples while are different on difficult samples.  $\mathcal{C}$  measures how the consistency of the segmentation maps between  $\hat{r}^p$  and  $\hat{r}^c$ .

we train the Relation U-Net with two different input images independently sampled from the training set and the four outputs are predicted independently. Thus, the estimations of the *Possible*  $\hat{r}^p$  and *Consensus*  $\hat{r}^c$  are not exactly the same given the same input since they are independently predicted by different sub-networks of the Relation U-Net. We compute the discrepancy between the estimation of  $\hat{r}^p$  and  $\hat{r}^c$  by:  $\mathcal{C} = \mathcal{D}(\hat{r}^p, \hat{r}^c)$ , where  $\mathcal{D}$  is a distance metric to measure the difference between two estimated segmentation maps of  $\hat{r}^p$  and  $\hat{r}^c$ . In this paper, we use the Dice coefficient as the distance metric to measure the difficulty to segment each image, defined as:  $\mathcal{C} = 2|\hat{r}^p \cap \hat{r}^c|/(\hat{r}^p + \hat{r}^c)$ , where  $\mathcal{C}$  measures the consistency between the segmentation maps between  $\hat{r}^p$  and  $\hat{r}^c$ . Fig. 3 shows several images with the segmentation maps of the relations  $\hat{r}^p$  and  $\hat{r}^c$ . For difficult samples, the segmentation maps of these two relations are different because they are independently predicted by different sub-networks within the Relation U-Net, yielding a low  $\mathcal{C}$ . However, for easy samples, the segmentation maps of these two relations are almost same and the corresponding  $\mathcal{C}$  values are also high. Thus, the value of  $\mathcal{C}$  can be used to measure the difficulty of the test images which is correlated to the accuracy of the segmentation result. In this paper, we name the value of  $\mathcal{C}$  as the confidence score which can rank test images by difficulty without ground-truth.

**Table 1.** The Dice performance of U-Net and Relation U-Net on the four datasets when  $x_1 = x_2$ .

Dataset	U-Net [1]	Relation U-Net				
		$\hat{s}_1$	$\hat{s}_2$	$(\hat{s}_1 + \hat{s}_2)/2$	$\hat{r}^p$	$\hat{s}^c$
LiTS	91.97 $\pm$ 0.69	92.44 $\pm$ 0.61	92.42 $\pm$ 0.91	92.62 $\pm$ 0.72	<b>92.78</b> $\pm$ 0.74	91.78 $\pm$ 0.83
Hippocampus	82.76 $\pm$ 0.42	82.88 $\pm$ 0.76	82.34 $\pm$ 0.56	82.59 $\pm$ 0.65	<b>83.24</b> $\pm$ 0.48	78.60 $\pm$ 0.74
BraTS	82.63 $\pm$ 0.97	82.91 $\pm$ 0.88	82.96 $\pm$ 0.83	83.27 $\pm$ 0.86	<b>84.24</b> $\pm$ 0.78	80.92 $\pm$ 1.16
ISIC	87.89 $\pm$ 0.53	87.36 $\pm$ 0.68	87.47 $\pm$ 0.56	<b>87.93</b> $\pm$ 0.54	86.08 $\pm$ 0.97	86.33 $\pm$ 0.84

### 3. EXPERIMENTAL RESULTS

#### 3.1. Datasets

We use four public datasets to evaluate the proposed method, including LiTS [6], Hippocampus [7], BraTS [8] and ISIC [9]. The LiTS dataset contains contrast-enhanced CT images. The Hippocampus dataset contains MRI images with the anterior and posterior of the hippocampus. For BraTS, we use the brain MRIs on 2018 Brain Tumor Segmentation (BraTS) challenges [8] with four different modalities (T1, T1ce, T2 and FLAIR). The ISIC contains dermoscopic images with skin cancer lesions. We use five-fold cross-validation strategy: all datasets are randomly split into five folds. Each time, one fold is used for testing and the rest of four folds are used for training. Average accuracy and standard deviation are reported.

#### 3.2. Implementation details

We follow the common strategy to train the neural network without loss of generality. Specifically, the Relation U-Net is trained by the Adam optimizer with the cross-entropy loss. The initial learning rate is set to 0.0001, and reduces to half at every 20 epochs in the total 100 training epochs. For Relation U-Net, we randomly sample two images on the training set during training. The ground-truth of the Possible and Consensus is computed based on the ground-truth of the input images for training. For evaluation, we use the common Dice Similarity Coefficient (DSC) [2, 4].

#### 3.3. Accuracy of Relation U-Net

##### 3.3.1. Accuracy of Relation U-Net when the input images sampled from the same image

Table 1 shows the Dice values of the vanilla U-Net (baseline) and the proposed Relation U-Net with estimated outputs of  $s_1$  and  $s_2$  and their relations  $r^p$  and  $r^c$ .  $(s_1 + s_2)/2$  denotes the average of the  $s_1$  and  $s_2$  in the testing when the input images  $x_1$  and  $x_2$  are sampled from the same input. Two observations can be obtained: (1) The output  $r^p$  provides higher Dice scores than U-Net on LiTS, Hippocampus, and BraTS and the average of  $(s_1 + s_2)/2$  provides higher Dice score than U-Net on ISIC. The results indicate that the Relation U-Net can learn the sub-networks for estimating the segmentation maps

**Table 2.** Comparison of Relation U-Net with other baselines.

Dataset	U-Net [1]		Relation U-Net		
	Baseline	Dropout [10]	$x_1 = x_2$	$x_2 \in \text{Train}$	$x_2 \in \text{Test}$
			$(\hat{s}_1 + \hat{s}_2)/2$	$\hat{s}_1$	$\hat{s}_1$
LiTS	91.97 $\pm$ 0.69	92.16 $\pm$ 0.80	92.62 $\pm$ 0.72	92.58 $\pm$ 0.64	<b>92.84</b> $\pm$ 0.39
Hippocampus	82.76 $\pm$ 0.42	82.63 $\pm$ 0.60	82.59 $\pm$ 0.65	<b>83.12</b> $\pm$ 0.62	<b>83.12</b> $\pm$ 0.63
BraTS	82.63 $\pm$ 0.97	82.73 $\pm$ 1.02	82.27 $\pm$ 0.86	<b>83.37</b> $\pm$ 0.95	83.36 $\pm$ 0.92
ISIC	87.89 $\pm$ 0.53	87.73 $\pm$ 0.66	87.93 $\pm$ 0.54	88.00 $\pm$ 0.51	<b>88.01</b> $\pm$ 0.52

and their relations of different input images. (2) From the table 1, we can see that the accuracy of the Possible relation  $r^p$  is higher than the accuracy of the Consensus relation  $r^c$ , indicating that these two relations capture different information for segmentation obtained by the different sub-networks of the Relation U-Net.

##### 3.3.2. Accuracy of Relation U-Net when the input images sampled from the different images

In this section, we evaluate the performance of the input  $x_1$  given the input image  $x_2$  which is sampled from training set (denoted as  $x_2 \in \text{train}$ ) and testing set (denoted as  $x_2 \in \text{test}$ ). In this scenario, the input  $x_2$  can be considered as the anchor and the different segmentation outputs  $s_1$  can be obtained by varying the choice of the anchor  $x_2$ . For each input image  $x_1$ , we randomly select 200 different images as the second input  $x_2$  and the average results are reported. We also compare it with the Dropout which trains the sub-networks during training by randomly dropping some neurons. For the vanilla U-Net, different segmentation maps can be obtained by applying the Monte Carlo (MC) Dropout on test images, similar to study [10]. We first train a U-Net with a dropout on the last layer and then take the MC samples of the prediction using the dropout during testing. We set  $n = 200$  and it also requires 200 forward passes for the same input image. Table 2 shows the results of different models on the four datasets. The segmentation accuracy of the Relation U-Net with different input images is slightly higher than the one with the input images sampled from the same image. The results indicate that the ensemble results of different pairs of input images can provide a robust segmentation. Finally, the Relation U-Net provides higher accuracies than the Vanilla U-Net (baseline) and U-Net with dropout.

#### 3.4. Correlation between the accuracy and confidence score $\mathcal{C}$

This section presents the results of the correlation between the accuracy of the segmentation and the corresponding estimated confidence score  $\mathcal{C}$ . We also compare the proposed  $\mathcal{C}$  with the one computed based on the vanilla U-Net with Dropout where different segmentation maps can be obtained by applying the MC Dropout [10] on test images with  $n = 200$  forward passes. Following study [11], the Possible relation of

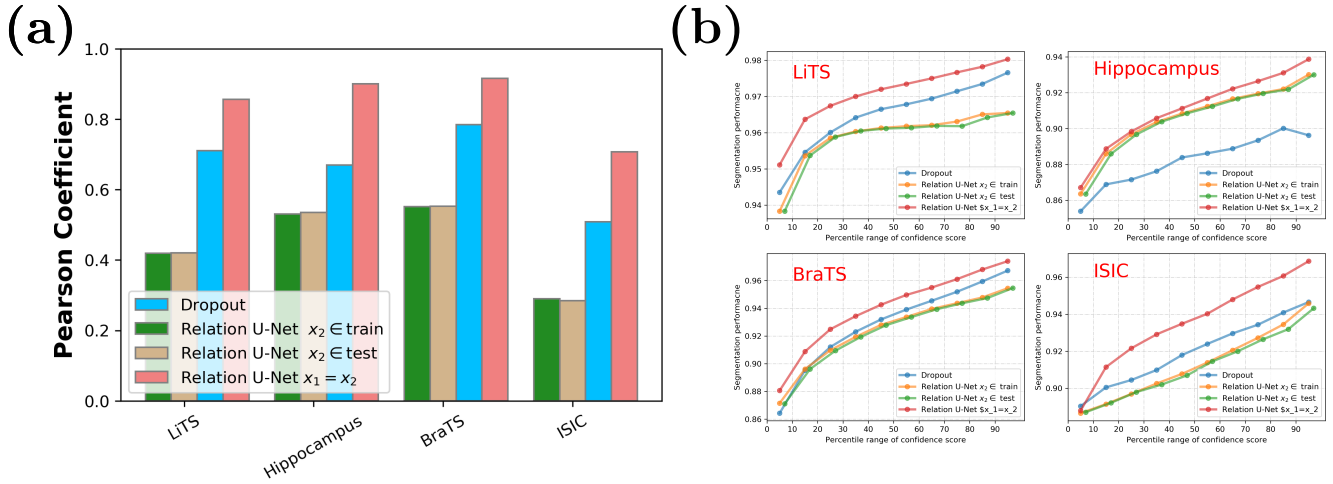


**Fig. 4.** (a) Comparison of the Pearson coefficient between the segmentation accuracy and confidence scores. (b) The segmentation accuracy (y-axis) for the test images thresholded by the confidence score (x-axis). The results are computed by the average over the five-fold cross-validation. On the test images without ground-truth, the segmentation accuracy increases with an increase in confidence scores.

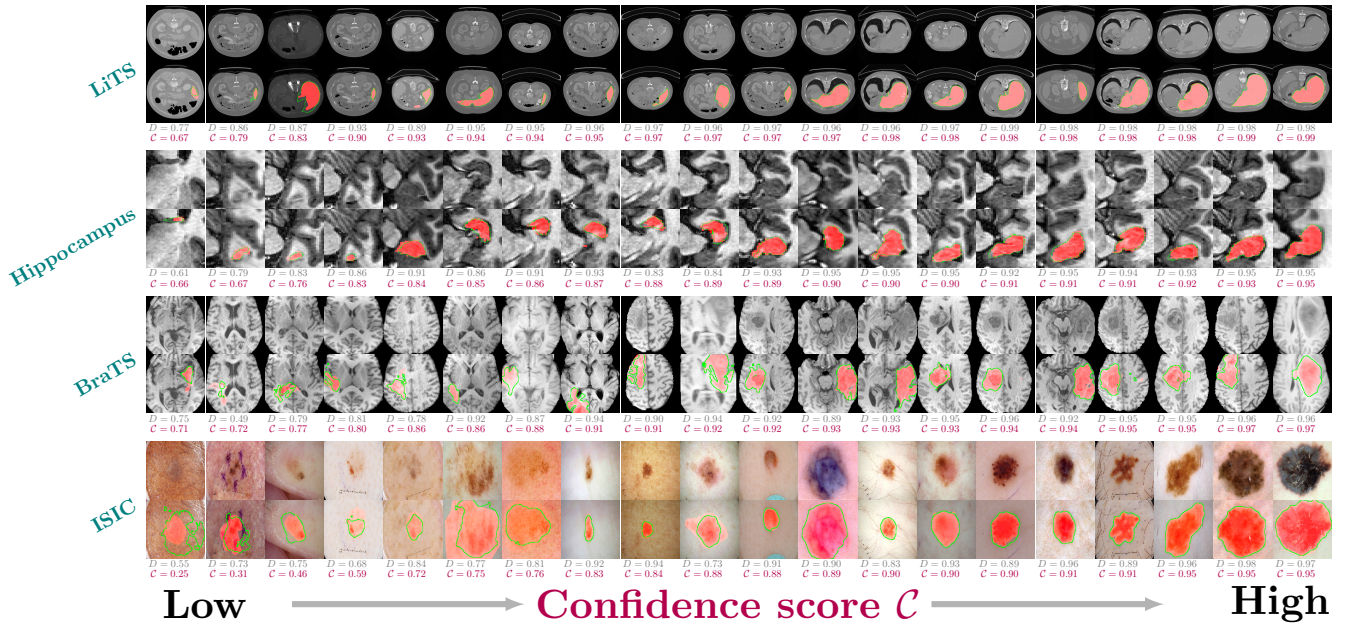


**Fig. 5.** Examples of the images (the first row on each data set) and their corresponding segmentation results (the second row on each dataset) ranked by the confidence score  $C$ . The red masks denote the ground-truth and the green contours denote the segmentation results. The Dice similarity coefficient  $D$  and confidence score  $C$  are shown under each example.

the  $n$  different segmentation maps is computed as:  $\hat{r}^P = \cup s_i$  and the Consensus relation is computed as:  $\hat{r}^c = \cap s_i$  where  $\cup$  and  $\cap$  are the operations of the union and intersection, respectively.

Fig. 4(a) shows the Pearson coefficients of different models which is computed between the confidence scores and the segmentation accuracies on the testing samples. It shows

that the Pearson coefficient of the proposed Relation U-net are higher than ones of other three methods across the four datasets. To test the discriminative of the confidence score, we plot the segmentation accuracy of test samples bucketed by the decile of confidence score [3]. We first rank all testing samples based on the estimated confidence score and the testing samples within the  $d\%$  percentile are included to compute

the accuracy of the segmentation. This is similar to the coverage [12, 13] which rejects the (100-d)% difficult samples for further attention. Fig. 4(b) shows the curves with different d% obtained by the Relation U-Net with the input images sampled from the same image  $x_1 = x_2$ . We show that examples at the highest percentiles on the rank often have high segmentation accuracy. Fig. 4(b) shows that when the ground truth is not available, we can still use the proposed confidence score to find difficult-to-segment samples. The remaining relatively easier-to-segment cases do enjoy a higher segmentation accuracy once the ground-truth is available. Overall, the confidence score provides an informative metric to evaluate segmentation accuracy when the ground-truth is not available.

Fig. 5 visualizes test images and their corresponding segmentation results ranked by the confidence scores. Images with low confidence scores tend to have small target regions, smooth boundaries and poor contrast between the target and background tissues. The accuracies of their segmentation results are usually low. Images with high confidence scores often have large target regions and clear boundaries, yielding more consistent segmentation maps of the Possible and Consensus relations.

#### 4. CONCLUSION

This paper proposed a simple generalization of the segmentation neural network which can not only provide the segmentation result, but also an estimated confidence score to evaluate segmentation accuracies for each test image when the ground-truth is not available. The segmentation network receives multiple two input images and outputs multiple outputs four different segmentation maps including the two segmentation maps of each input image as well as the two relations among the pairwise of input images. Our proposed method can provide better results than the baseline and can also provide a confidence score for ranking the test images by difficulty without ground-truth.

#### 5. REFERENCES

- [1] Olaf Ronneberger, Philipp Fischer, and Thomas Brox, "U-Net: Convolutional networks for biomedical image segmentation," in *MICCAI 2015*, 2015, pp. 234–241.
- [2] Alireza Mehrtash, William M Wells, Clare M Tempany, Purang Abolmaesumi, and Tina Kapur, "Confidence calibration and predictive uncertainty estimation for deep medical image segmentation," *IEEE TMI*, vol. 39, no. 12, 2020.
- [3] Chirag Agarwal, Daniel D'souza, and Sara Hooker, "Estimating example difficulty using variance of gradients," in *CVPR*, 2022, pp. 10368–10378.
- [4] Renzhen Wang, Shilei Cao, Kai Ma, Yefeng Zheng, and Deyu Meng, "Pairwise learning for medical image segmentation," *MIA*, vol. 67, pp. 101876, 2021.
- [5] Sheng He, Yanfang Feng, P Ellen Grant, and Yangming Ou, "Deep relation learning for regression and its application to brain age estimation," *IEEE TMI*, vol. 41, no. 9, pp. 2304–2317, 2022.
- [6] Patrick ilic, Patrick Christ, Hongwei Bran Li, Eugene Vorontsov, Avi Ben-Cohen, Georgios Kaissis, Adi Szeskin, Colin Jacobs, Gabriel Efrain Humpire Mamani, Gabriel Chartrand, et al., "The liver tumor segmentation benchmark (LIST)," *MIA*, vol. 84, pp. 102680, 2023.
- [7] Michela Antonelli, Annika Reinke, Spyridon Bakas, Keyvan Farahani, Annette Kopp-Schneider, Bennett A Landman, Geert Litjens, Bjoern Menze, Olaf Ronneberger, Ronald M Summers, et al., "The medical segmentation decathlon," *Nature communications*, vol. 13, no. 1, pp. 4128, 2022.
- [8] Bjoern H Menze, Andras Jakab, Stefan Bauer, Jayashree Kalpathy-Cramer, Keyvan Farahani, Justin Kirby, Yuliya Burren, Nicole Porz, Johannes Slotboom, Roland Wiest, et al., "The multimodal brain tumor image segmentation benchmark (brats)," *IEEE TMI*, vol. 34, no. 10, pp. 1993–2024, 2014.
- [9] Noel Codella, Veronica Rotemberg, Philipp Tschandl, M Emre Celebi, Stephen Dusza, David Gutman, Brian Helba, Aadi Kalloo, Konstantinos Liopyris, Michael Marchetti, et al., "Skin lesion analysis toward melanoma detection 2018: A challenge hosted by the international skin imaging collaboration (ISIC)," *arXiv preprint arXiv:1902.03368*, 2019.
- [10] Tanya Nair, Doina Precup, Douglas L Arnold, and Tal Arbel, "Exploring uncertainty measures in deep networks for multiple sclerosis lesion detection and segmentation," *MIA*, vol. 59, pp. 101557, 2020.
- [11] Leo Joskowicz, D Cohen, N Caplan, and Jacob Sosna, "Automatic segmentation variability estimation with segmentation priors," *MIA*, vol. 50, pp. 54–64, 2018.
- [12] Florin C Ghesu, Bogdan Georgescu, Awais Mansoor, Youngjin Yoo, Eli Gibson, RS Vishwanath, Abishek Balachandran, James M Balter, Yue Cao, Ramandeep Singh, et al., "Quantifying and leveraging predictive uncertainty for medical image assessment," *MIA*, vol. 68, pp. 101855, 2021.
- [13] Sheng He, Yanfang Feng, P Ellen Grant, and Yangming Ou, "Segmentation ability map: Interpret deep features for medical image segmentation," *MIA*, vol. 84, pp. 102726, 2023.